OPEN ACCESS Freely available online

PLOS ONE

A Mathematical Model for MicroRNA in Lung Cancer

Hye-Won Kang[1☯], Melissa Crawford[2], Muller Fabbri[3], Gerard Nuovo[2], Michela Garofalo[3], S. Patrick Nana-Sinkam[2*☯], Avner Friedman[1,4☯]

1 Mathematical Biosciences Institute, Ohio State University, Columbus, Ohio, United States of America, **2** Davis Heart and Lung Research Institute, Ohio State University, Columbus, Ohio, United States of America, **3** Department of Molecular Virology, Immunology and Medical Genetics, Ohio State University, Columbus, Ohio, United States of America, **4** Department of Mathematics, Ohio State University, Columbus, Ohio, United States of America

Abstract

Lung cancer is the leading cause of cancer-related deaths worldwide. Lack of early detection and limited options for targeted therapies are both contributing factors to the dismal statistics observed in lung cancer. Thus, advances in both of these areas are likely to lead to improved outcomes. MicroRNAs (miRs or miRNAs) represent a class of non-coding RNAs that have the capacity for gene regulation and may serve as both diagnostic and prognostic biomarkers in lung cancer. Abnormal expression patterns for several miRNAs have been identified in lung cancers. Specifically, let-7 and miR-9 are deregulated in both lung cancers and other solid malignancies. In this paper, we construct a mathematical model that integrates let-7 and miR-9 expression into a signaling pathway to generate an in silico model for the process of epithelial mesenchymal transition (EMT). Simulations of the model demonstrate that EGFR and Ras mutations in non-small cell lung cancers (NSCLC), which lead to the process of EMT, result in miR-9 upregulation and let-7 suppression, and this process is somewhat robust against random input into miR-9 and more strongly robust against random input into let-7. We elected to validate our model in vitro by testing the effects of EGFR inhibition on downstream MYC, miR-9 and let-7a expression. Interestingly, in an EGFR mutated lung cancer cell line, treatment with an EGFR inhibitor (Gefitinib) resulted in a concentration specific reduction in c-MYC and miR-9 expression while not changing let-7a expression. Our mathematical model explains the signaling link among EGFR, MYC, and miR-9, but not let-7. However, very little is presently known about factors that regulate let-7. It is quite possible that when such regulating factors become known and integrated into our model, they will further support our mathematical model.

Citation: Kang H-W, Crawford M, Fabbri M, Nuovo G, Garofalo M, et al. (2013) A Mathematical Model for MicroRNA in Lung Cancer. PLoS ONE 8(1): e53663. doi:10.1371/journal.pone.0053663

Editor: Elad Katz, University of Edinburgh, United Kingdom

Received May 31, 2012; **Accepted** December 3, 2012; **Published** January 24, 2013

Funding: This research has been supported in part by the Mathematical Biosciences Institute and the National Science Foundation under grant DMS 0931642 and by the National Cancer Institute under grant CA 150297. The funders had no role in study design, data collection and analysis, decision to publish, or preparation of the manuscript.

Competing Interests: The authors have declared that no competing interests exist.

* E-mail: Patrick.Nana-Sinkam@osumc.edu

☯ These authors contributed equally to this work.

Introduction

Lung cancer is the leading cause of cancer-related deaths worldwide. In the U.S. the number of new occurrences is approximately 230,000 annually, and the number of deaths is 160,000, representing 25% of all cancer related deaths [1]. Lack of early detection and limited options for target therapies are both contributing factors to the dismal statistics observed in lung cancer. Thus, advances in both of these areas are likely to lead to improved outcomes.

microRNAs (miRs or miRNAs) represent a class of non-coding RNAs that have the capacity for gene regulation and may serve as diagnostic and prognostic biomarkers in lung cancer. Abnormal expression patterns for miRNAs have been identified in lung cancers. Specifically, let-7 and miR-9 are deregulated in both lung cancers and other solid malignancies. Takamizawa et al. (2004) and Nicoloso et al. (2009) demonstrated that let-7 is downregulated in non-small cell lung cancers (NSCLC) [2,3]. Several investigators have shown that let-7 harbors tumor suppressive properties both in vitro and in vivo [4,5]. Using microarray data, Yanaihara et al. (2006) reported that miR-9 was decreased in NSCLC [6], whereas Volinia et al. (2006) reported an increase in miR-9 expression [7]. More recently Crawford et al. (2009) reported increased expression of miR-9 in NSCLC [8], and Võsa et al. (2011) drew the same conclusion from their microarray data [9]. Recently, we have also independently analyzed 140 cases of NSCLC and compared miR-9 expression between tumors and adjacent uninvolved lung tissue. We found that in approximately 130 cases miR-9 was overexpressed in lung tumors; see Supplementary Material S1. A recent investigation showed that miR-9 contributes to metastatic potential in breast cancer in part by targeting components of epithelial mesenchymal transition (EMT) [10]. However, the role for miR-9 in the pathogenesis of lung cancer is less well understood. Mascaux et al. (2009) demonstrated an induction in miR-9 expression during bronchial squamous carcinogenesis [11].

Given the fact that a single miRNA may regulate tens to hundreds of genes, understanding the importance of an individual miRNA in cancer biology can be challenging. This is further complicated by observations that the dysregulation of several miRNAs is often required to cause a given phenotype. To date, few models exist to elucidate the mechanisms by which multiple miRNAs contribute both individually and in tandem to promote

tumor initiation and progression. Applying mathematical modeling to miRNA biology provides an opportunity to understand these complex relationships. In the current study, we have developed for the first time a mathematical model focusing on miRNAs (miR-9 and let-7) in the context of lung cancer as a model system; however, our model system could be applicable to miRNA biology in both malignant and benign diseases. For simplicity, we have integrated these miRNAs into a signaling pathway to generate an in silico model for the process of EMT. Herein, we include the EGF-EGFR complex and associated downstream signaling culminating in matrix metalloproteinase (MMP) expression. Other components of our pathway include SOS, Ras, ERK, MYC,E-Cadherin, miR-9, and let-7.

We have simulated the model under several scenarios of gene mutations that may lead to lung cancer and determined, in each scenario, that miR-9 was upregulated and let-7 downregulated. We have also shown that the process leading to EMT is somewhat robust against random input into miR-9 and more strongly robust against random input into let-7.

Results

Biological Background

Figure 1 A shows a signaling pathway involving miR-9, let-7, MYC, and EMT, while Figure 1 B is a simplified version that will be used in the mathematical model. miR-9 is upregulated in NSCLC. Although Yanaihara et al. (2006) reported a decrease of miR-9 using microarray data [6], several other papers, some more recent, reported an increase of miR-9 in NSCLC: Volinia et al. (2006) and Võsa et al. (2011) used microarray [7,9], and Crawford et al. (2009) used PCR [8]. We have analyzed 140 cases of NSCLC with PCR and demonstrate miR-9 overexpression in lung tumors compared to adjacent uninvolved lung and present a representation of 30 such cases; see Supplementary Material S1.

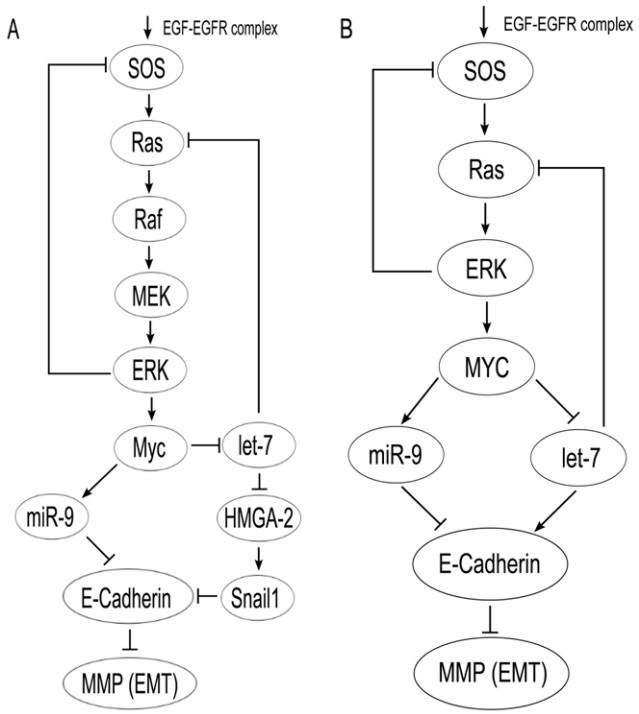

Figure 1. A signaling pathway for lung cancer. A pathway from EGF-EGFR complex to MMP, which includes miR-9 and let-7, is given in (A) and a simplified pathway is shown in (B).
doi:10.1371/journal.pone.0053663.g001

MYC controls many fundamental cellular processes, and aberrant MYC expression is known to be associated with cancer. For example, Frenzel et al. (2010) observed that MYC is usually activated in many cancers [12], and Aguda et al. (2008) showed how MYC can act as either an oncogene or tumor suppressor [13]. In lung cancer, MYC family oncogenes are amplified in both small-cell lung cancers (SCLC) and NSCLC [14,15]. Moreover, c-MYC can induce metastasis in c-Raf mutant NSCLC [16].

Investigators have also identified a link between MYC and miRNAs that also play a significant role in cancer. Rinaldi et al. (2007) showed that both MYC and the miRNA cluster miR-17-92 are amplified in human mantle cell lymphoma [17]; Frenzel et al. (2010) described miR-9 as an oncogenic miRNA and let-7 as a tumor suppressor miRNA both of which are regulated by MYC [12]: MYC induces miR-9, which blocks tumor suppressor pathways, while MYC inhibits let-7, which blocks oncogenic pathways. Ma et al. (2010) found that miR-9 is driven by MYC, downregulates E-Cadherin, and induces metastasis in breast cancer [10]. Wolfer and Ramaswamy (2011) investigated the role of MYC in breast cancer metastasis using a signaling pathway that includes let-7, miR-9, E-Cadherin, and EMT [18].

Our proposed pathway is based on several lines of investigation. Similar to breast cancer, let-7 is downregulated in NSCLC [2,3]. Takamizawa et al. (2004) demonstrated that reductions of let-7 as high as 80% occurred in tumors compared to uninvolved adjacent lung tissue [2]. In this same study, only $7/16$ cases had such reductions ($N=16$). However, more recent investigation by Inamura et al. (2007) demonstrated that among well-differentiated adenocarcinomas ($N=26$), the reductions in let-7 family members were more modest (approximately $35-40\%$) [19]. Wang et al. (2011) asserted that c-MYC represses transcription of let-7 [20]. Johnson et al. (2005) and others showed that Ras is suppressed by let-7 [21]. Lee and Dutta (2007) suggested that let-7 represses HMGA-2 in a lung cancer cell [22], and Thuault et al. (2008) asserted that HMGA-2 causes EMT by activating Snail1 which in turn represses E-Cadherin [23]. E-Cadherin downregulates MMP in bronchial tumor cells [24]. Both E-Cadherin and MMP have been implicated as biomarkers in several solid malignancies including lung cancer. A recent investigation showed that elevated levels of MMP-9 in cases of NSCLC correlated with advanced stages and the presence of metastases [25]. In addition Rao et al. (2005) demonstrated in vitro and in vivo that adenoviral mediated gene transfer of MMP-9 could reduce lung cancer invasive capacity and formation of metastases [26]. Decreased E-Cadherin expression also appears to correlate with clinically more aggressive disease [27–29].

Roberts and Der (2007) used an EGFR-Ras-Raf-MEK-ERK pathway to explain that 10% of NSCLC arise from EGFR mutations and that 30% of NSCLC arise from mutations in Ras [30]. SOS is an intermediate between the EGF-EGFR complex and Ras [31], and is repressed through negative feedback by ERK [32,33]. Huang et al. (2011) showed that ERK/MAPK in lung cancer activates c-MYC [34]. Figure 1 A provides a summary of the above lines of investigation. For the purposes of simplicity, we propose a simpler version in Figure 1 B which nevertheless encompasses the main features of Figure 1 A. We recognize that other signaling pathways are driven by the EGF-EGFR complex including PI3K/Akt which regulates cell survival. However, given our interest in miR-9 and let-7 as potential biomarkers, we have not included this pathway in our model.

Model Equations

We introduce a system of ordinary differential equations that describe a signaling pathway of EMT (represented by the level of MMP mRNA) induced by MYC through miR-9 and let-7 as shown in Figure 1 B. The differential equations (1)−(8) are based on Figure 1 B, and detailed explanations are given in Methods. Notation for species concentrations is given in Table 1.

$$\frac{dS}{dt}=\mu_S E\cdot\frac{S_{tot}-S}{S_{tot}-S+K_{S1}}-\delta_S Ek\cdot\frac{S}{S+K_{S2}} \quad (1)$$

$$\frac{dR}{dt}=\mu_R S\cdot\frac{R_{tot}-R}{R_{tot}-R+K_{R1}}\cdot\frac{K_{R2}}{L+K_{R2}}-\delta_R\cdot\frac{R}{R+K_{R3}} \quad (2)$$

$$\frac{dEk}{dt}=\mu_{Ek} R\cdot\frac{Ek_{tot}-Ek}{Ek_{tot}-Ek+K_{Ek1}}-\delta_{Ek}\cdot\frac{Ek}{Ek+K_{Ek2}} \quad (3)$$

$$\frac{dC}{dt}=\mu_C Ek-\delta_C C \quad (4)$$

$$\frac{dM}{dt}=\mu_M\cdot\frac{C^4}{C^4+K_M}-\delta_M M \quad (5)$$

$$\frac{dL}{dt}=\mu_L\cdot\frac{K_L}{C+K_L}-\delta_L L \quad (6)$$

$$\frac{dH}{dt}=\mu_H L\cdot\frac{K_H}{M+K_H}-\delta_H H \quad (7)$$

$$\frac{dP}{dt}=\mu_P-\delta_P P\cdot\frac{H}{H+K_P}. \quad (8)$$

Simulations

A large number of NSCLC cases arise from EGFR mutations [35,36] or Ras mutations [37]. We assume that negative feedback of ERK to SOS may be disrupted in NSCLC. We describe these aberrations by increasing E, increasing μ_R, or decreasing δ_S, so that concentration level of EGF-EGFR complex increases, Ras is over-activated by SOS, or negative feedback of ERK to SOS is weakened. The following simulations demonstrate the effect of increase in E and in μ_R and decrease in δ_S on the increase in miR-9, let-7 and MMP.

Simulations of the model equations were performed using Matlab. We used an ode solver, ode15 s, to solve a system of ordinary differential equations numerically. To solve a system of stochastic differential equations with random inputs in miR-9 or let-7 numerically, we developed a code using an Euler scheme. All initial values are taken to be those of healthy normal cells, namely, $S(0)=S_0$, $R(0)=R_0$, $Ek(0)=Ek_0$, $C(0)=C_0$, $M(0)=M_0$, $L(0)=L_0$, $H(0)=H_0$, and $P(0)=P_0$.

If E increases as a result of mutations in EGFR, we expect an increase in miR-9 and a decrease in let-7 as indeed are observed in lung cancer. There will also be an increase in MMP mRNA signifying EMT and cell migration, which contributes to metastasis. Figure 2 shows the level of miR-9, let-7, and MMP at $t=10^5$ min as a function of E/E_0: as E/E_0 increases, miR-9 and MMP mRNA concentrations increase and let-7 concentration decreases. For example, for $E/E_0=5$, the level of miR-9 increases by 11-fold from $1.7987\times10^{-5}\,\mu M$ to $2.0362\times10^{-4}\,\mu M$ and that of MMP mRNA concentration increases by 5-fold from $1.1569\times10^{-13}\,\mu M$ to $5.6252\times10^{-13}\,\mu M$ compared to the level in healthy normal cells. On the other hand, the level of let-7 concentration decreases by 1.4-fold from $0.0023\,\mu M$ to $0.0016\,\mu M$.

Figure 3 shows the effect of Ras mutations on the levels of miR-9, let-7, and MMP mRNA after 10^5 min. Ras mutations are represented by an increase in μ_R/μ_{R0}. We see that as μ_R/μ_{R0} increases, so do the concentrations of miR-9 and MMP mRNA while let-7 concentration decreases. For example, for $\mu_R/\mu_{R0}=5$, the level of miR-9 concentration increases by 17-fold from $1.7987\times10^{-5}\,\mu M$ to $3.0210\times10^{-4}\,\mu M$ and that of MMP mRNA concentration increases by 7-fold from $1.1569\times10^{-13}\,\mu M$ to $8.3569\times10^{-13}\,\mu M$ compared to the level in healthy normal cells. On the other hand, the level of let-7 concentration decreases by 1.5-fold from $0.0023\,\mu M$ to $0.0015\,\mu M$.

When the negative feedback of ERK to SOS is weakened as a result of possible mutations in ERK, the parameter δ_S in Eq. (1) is decreased. Figure 4 shows the effect of these mutations: as δ_S/δ_{S0} decreases, the concentrations of miR-9 and MMP increase and that of let-7 decreases. For example, for $\delta_S/\delta_{S0}=1/2$, the level of miR-9 concentration increases by 3-fold from $1.7987\times10^{-5}\,\mu M$ to $5.6205\times10^{-5}\,\mu M$ and that of MMP mRNA concentration increases by 2-fold from $1.1569\times10^{-13}\,\mu M$ to $1.9674\times10^{-13}\,\mu M$ compared to the level in healthy normal cells. On the other hand, the level of let-7 concentration decreases by 1.2-fold from $0.0023\,\mu M$ to $0.0020\,\mu M$.

In Figure 5, we simulate the time evolution of SOS, Ras, ERK, MYC, miR-9, let-7, E-Cadherin, and MMP mRNA over a period of $t=1$ min with $E=10E_0$; in Figure 6 the simulations are carried out for the longer period of 10^5 min. A comparison between the panels of the two figures shows that the dynamics of SOS, Ras, and ERK are very fast; MYC, miR-9, and let-7 change relatively slower, and MMP mRNA takes even longer to reach equilibrium. After 10^5 minutes, SOS and Ras increased by 3-fold from

Table 1. Notation for species concentrations.

Notation	Description
E	EGF-EGFR complex (constant)
S	active SOS concentration
R	active Ras concentration
Ek	active ERK concentration
C	MYC protein concentration
M	miR-9 concentration
L	let-7 concentration
H	E-Cadherin concentration
P	MMP mRNA concentration

The table gives notation for species concentrations that are used in the mathematical model.
doi:10.1371/journal.pone.0053663.t001

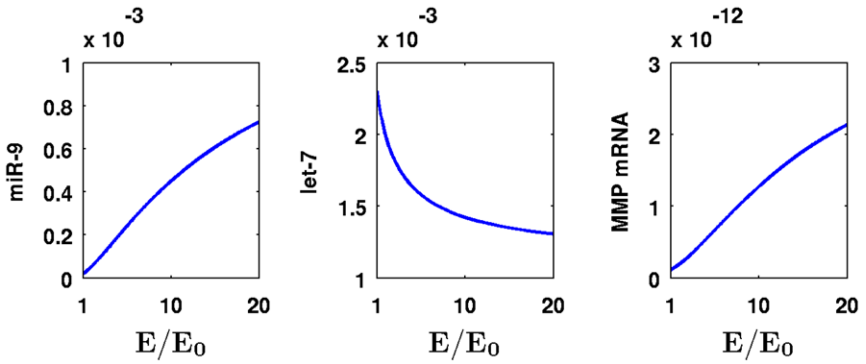

Figure 2. Concentration changes of miR-9, let-7, and MMP mRNA with different values for E. The units on the vertical axes are in μM and the time is at $t=10^5$ min.
doi:10.1371/journal.pone.0053663.g002

$0.0298\,\mu M$ to $0.0924\,\mu M$ and from $0.0053\,\mu M$ to $0.0169\,\mu M$, respectively; ERK and MYC increased by 2-fold from $0.2746\,\mu M$ to $0.6076\,\mu M$ and from $0.2189\,\mu M$ to $0.4840\,\mu M$, respectively; miR-9 increased by 24-fold from $1.8\times10^{-5}\,\mu M$ to $4.3035\times10^{-4}\,\mu M$; MMP increased by 10-fold from $1.1574\times10^{-13}\,\mu M$ to $1.2144\times10^{-12}\,\mu M$ compared to their values in normal cells; let-7 decreased by 1.6-fold from $0.0023\,\mu M$ to $0.0014\,\mu M$, and E-Cadherin decreased by 20-fold from $0.1\,\mu M$ to $0.005\,\mu M$.

Figures 7 and 8 show similar simulations when μ_R is increased to $10\mu_{R0}$ and Figures 9 and 10 show similar simulations when δ_S is decreased to $(1/10)\delta_{S0}$. In Figure 8, Ras increased by 4-fold from $0.0053\,\mu M$ to $0.0231\,\mu M$; ERK and MYC increased by 3-fold from $0.2746\,\mu M$ to $0.6998\,\mu M$ and from $0.2189\,\mu M$ to $0.5574\,\mu M$, respectively; miR-9 increased by 42-fold from $1.8\times10^{-5}\,\mu M$ to $7.5611\times10^{-4}\,\mu M$; MMP increased by 19-fold from $1.1574\times10^{-13}\,\mu M$ to $2.2358\times10^{-12}\,\mu M$ compared to their values in normal cells; SOS decreased by 2.3-fold from $0.0298\,\mu M$ to $0.0127\,\mu M$; let-7 decreased by 1.8-fold from $0.0023\,\mu M$ to $0.0013\,\mu M$, and E-Cadherin decreased by 38-fold from $0.1\,\mu M$ to $0.0026\,\mu M$. In Figure 10, concentration changes essentially in the same amount as in Figure 6.

It would be interesting to study the effect of a 'background' on miR-9 and let-7, namely, the genes with whom these miRNAs interact. Such interactions however, are not reported in the literature. We therefore model such interactions by a random input. Figure 11 shows how random perturbations of miR-9 affect MMP (EMT). Setting $E/E_0=10$ and $E/E_0=20$ as given in Figure 2, miR-9 perturbed by random Gaussian input and MMP are shown in Figure 11 A–D and E–H, respectively (we added $\sigma dB(t)$ on the right-hand side of (5) where $B(t)$ is a standard Brownian motion). Panels A/B and E/F in Figure 11 correspond to the case when miR-9 is perturbed by Gaussian input with $\sigma=10^{-5}$ and Panels C/D and G/H in Figure 11 correspond to the case when we increase σ to 1.2×10^{-5}. In Panels B/D/F/H in Figure 11, we compare MMP concentration with random perturbations (red line) and without perturbations (green dotted line). Figure 12 shows similar results in the case of let-7 with $\sigma=5\times10^{-5}$ and $\sigma=10^{-4}$. Panels A/B and E/F in Figure 12 correspond to the case when let-7 is perturbed by Gaussian input with $\sigma=5\times10^{-5}$ and Panels C/D and G/H in Figure 12 correspond to the case when we increase σ to 10^{-4}. Figures 13 and 14 show means (blue or red line) and standard deviations (black dotted line) from the means of miR-9, let-7, and MMP concentrations obtained from 1,000 realizations of simulation with the same parameters in Figures 11 and 12. Simulation results in Figures 11-14 are obtained with fixed time step, $\Delta t=0.005$ min.

We conclude that mean MMP concentrations and standard deviations from the means are stable (robust) to small perturbations in miR-9, i.e. when $\sigma=10^{-5}$. However, when we increase σ already to 1.2×10^{-5} stability of standard deviations from the mean MMP concentration tends to break down as we see from Panels D/H in Figure 13; Panels D/H in Figure 11 show one sample path of unstable MMP concentration against miR-9

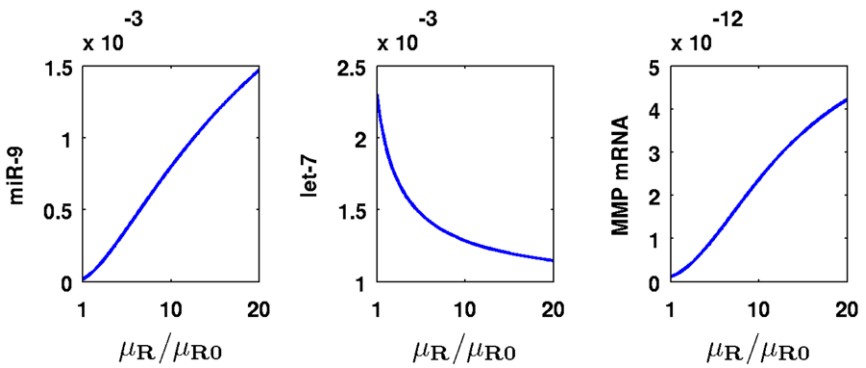

Figure 3. Concentration changes of miR-9, let-7, and MMP mRNA with different values for μ_R. The units on the vertical axes are in μM and the time is at $t=10^5$ min.
doi:10.1371/journal.pone.0053663.g003

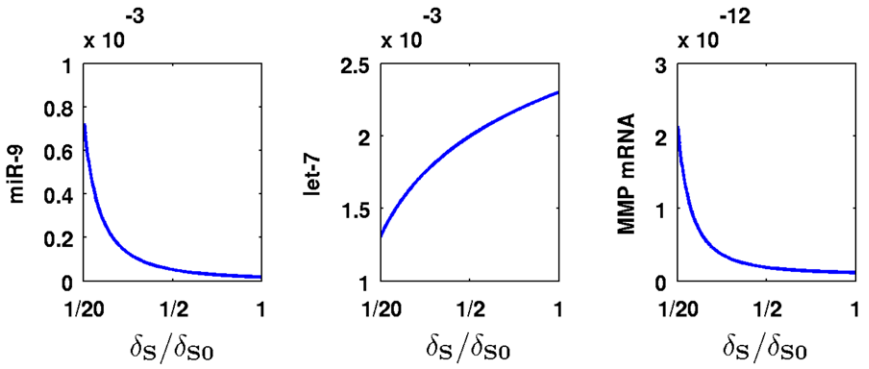

Figure 4. Concentration changes of miR-9, let-7, and MMP mRNA with different values for δ_s. The units on the vertical axes are in μM and the time is at $t = 10^5$ min.
doi:10.1371/journal.pone.0053663.g004

perturbation. On the other hand, mean MMP concentrations and standard deviations from the means are much more stable for let-7 perturbations with large σ, and trajectories of means closely follow the trajectory of MMP without random input as shown in Figure 14; Figure 12 shows one sample path of MMP concentration against let-7 perturbation. Notice that we have taken $\sigma = 5 \times 10^{-5}$ in Panels A/B/E/F and $\sigma = 10^{-4}$ in Panels C/D/G/H. For let-7, if we take σ as small as 1.2×10^{-5} as we did in Panels C/D/G/H in Figure 11, standard deviations are very small and negligible (not shown here). The reason why MMP is more stable against random perturbations of let-7 than against miR-9 perturbations is that let-7 perturbations undergo damping by the negative feedbacks from let-7 to Ras and from ERK to SOS, as shown in Figure 1. Similar results (not shown here) hold when we vary μ/μ_0 or δ_S/δ_{S0}, instead of E/E_0.

Sensitivity Analysis

Since we are focusing on miR-9 upregulation and let-7 downregulation as potential biomarkers for lung cancer, we wanted to determine how the quotient M/L of miR-9 divided by let-7 depends on the parameters of the model equations. We focused on the 14 parameters in Table 2 which are only

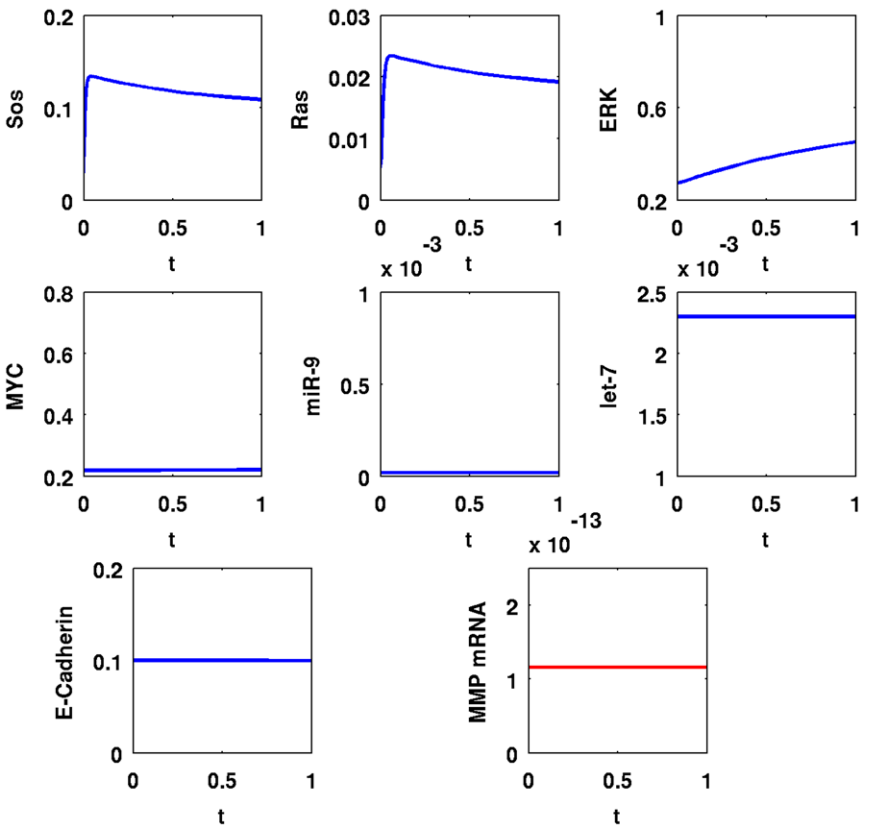

Figure 5. Simulation results for a cancer cell with EGFR mutations, $\mathbf{E} = 10\mathbf{E}_0$. Time is from $t = 0$ min to $t = 1$ min; initial values are those of a normal healthy cell; the units on the vertical axes are in μM and the units on the horizontal axes are in minutes.
doi:10.1371/journal.pone.0053663.g005

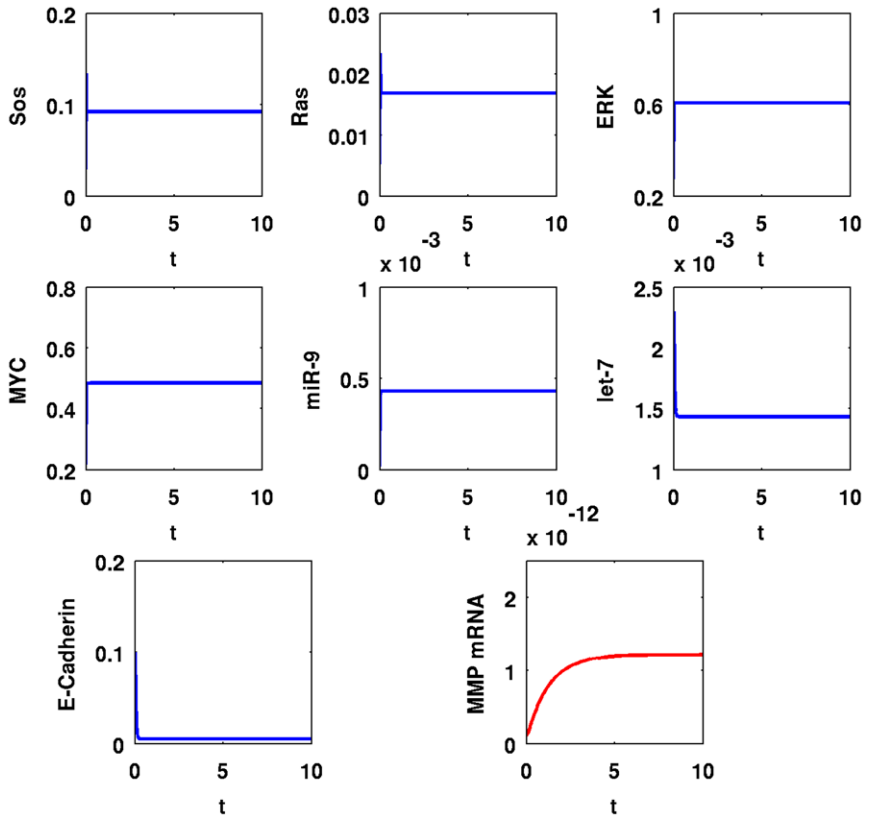

Figure 6. Simulation results for a cancer cell with EGFR mutations, $\mathbf{E}=10\mathbf{E}_0$. Time is from $t=0$ min to $t=10^5$ min; initial values are those of a normal healthy cell; the units on the vertical axes are in μM and the units on the horizontal axes are scaled in 10^4 minutes.
doi:10.1371/journal.pone.0053663.g006

estimations. We performed sensitivity analysis, employing the method of partial rank correlation coefficient (PRCC), using previously described program [38]. We let each of the 14 parameters vary in the interval between $1/2$ of the estimated value and twice its estimated value. Using Latin Hypercube sampling method as in [38], we sampled each parameter from uniformly distributed intervals and ran 2,000 realizations of simulation. Then, we transformed the sampled parameter values and the ratio M/L between miR-9 and let-7 as computed in the simulation to rank values, and computed partial rank correlation coefficients. PRCC values of the estimated parameters and their ranges are presented in Table 3, and scatter plots of statistically significant parameters are shown in Figure 15.

Among the 14 parameters, K_{R2}, K_M, K_L, μ_C, μ_M, and μ_L were statistically significant. The parameters μ_C and μ_M were strongly positively correlated with M/L. This is natural; indeed μ_C and μ_M are production rates of MYC and miR-9. As we increase production rate of MYC, miR-9 concentration increases and let-7 concentration decreases. On the other hand, μ_L, K_M, and K_L were strongly negatively correlated to M/L. This is also to be expected. Indeed, μ_L is the production rate of let-7, K_M is the saturation constant of MYC as source for miR-9, and K_L is the control constant of MYC in the let-7 equation. Therefore, it is natural that M/L would decrease as the parameters μ_L, K_M, and K_L increase. When we ran 10,000 realizations of simulation, we obtained similar results.

EGFR inhibition reduces both c-MYC and miR-9 in a concentration dependent manner

In an initial attempt to validate our mathematical model, we treated an EGFR mutant lung cancer cell line with several concentration of the clinically used EGFR inhibitor Gefitinib. We then assessed treated cells for miR-9, let-7a and c-MYC expression by QRT-PCR. As shown in Figure 16, we determined that while lower concentrations ($1\,\mu M$) of Gefitinib caused a statistically significant reduction in both miR-9 and c-MYC, similar effects were not evident at higher concentrations of Gefitinib or in let-7a. These findings while they would need to be validated in other cell lines suggest the additional complexity of the effects EGFR inhibition on miRNA expression and that our mathematical model only partially predicts the biological links between EGFR, c-MYC and miRNA in lung cancer.

Discussion

Lung cancer is the leading cause of cancer-related deaths worldwide. The majority of cases are diagnosed at later stages thus limiting therapeutic options and contributing to poor outcome. As a result, investigators have sought to identify lung cancer specific biomarkers that may be utilized for early detection and to better understand the metastatic process. Such biomarkers may significantly improve prognosis and reduce mortality. In this paper, we have proposed a mathematical model that integrates the miRNAs let-7 and miR-9 into the process of EMT. miR-9 has been shown

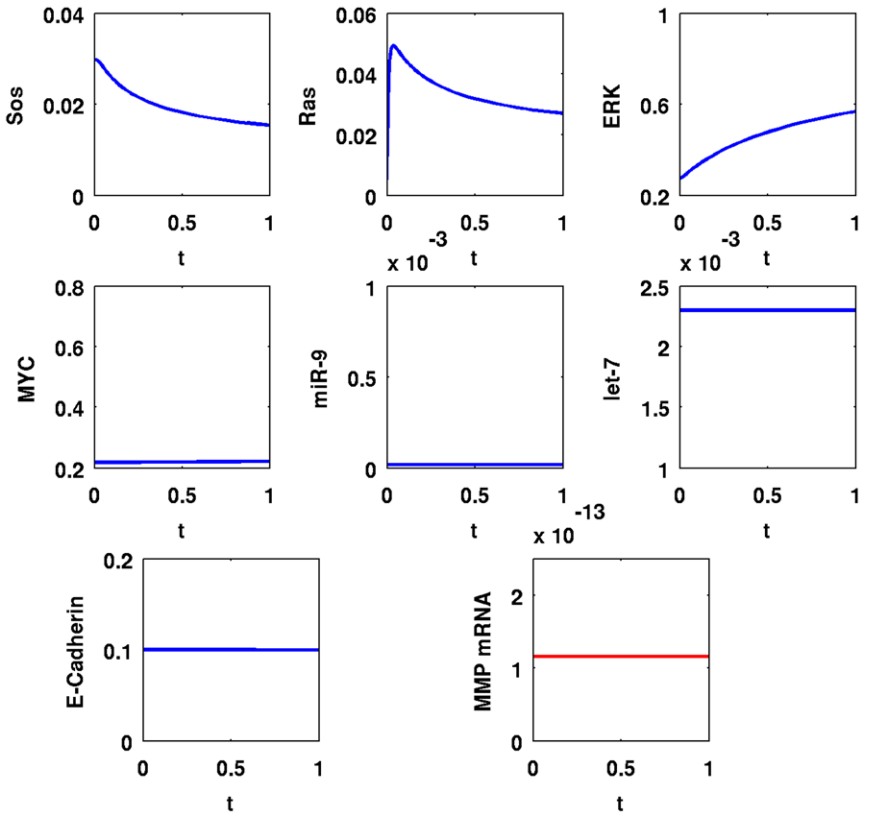

Figure 7. Simulation results for a cancer cell with Ras mutations, $\mu_R = 10\mu_{R0}$**.** Time is from $t = 0$ min to $t = 1$ min; initial values are those of a normal healthy cell; the units on the vertical axes are in μM and the units on the horizontal axes are in minutes.
doi:10.1371/journal.pone.0053663.g007

to be significantly upregulated and let-7 downregulated in NSCLC.

Based on the experimental literature, we introduced a signaling pathway from the EGF-EGFR complex to MMP expression which involves SOS, Ras, ERK, MYC, the miRNAs miR-9 and let-7, E-Cadherin, and MMP. Recent studies have demonstrated elevated MMP-9 in NSCLC [25], but for modeling purposes we have referred to MMP in a generic manner. Using an EGFR mutant lung cancer cell line, we showed that inhibition of EGFR leads to a reduction in miR-9 as well as c-MYC expression. However, the relationships between miR-9 and c-MYC were not consistent at higher concentrations of drug treatment. These findings support the complexity of the kinetics of miRNA and target gene relationships and highlight the inherent difficulties with modeling miRNA biology. Our findings suggest that higher concentrations of EGFR are likely to engage other regulators of miR-9 and/or c-MYC and that miR-9 may be under the regulatory control of additional genes beyond c-MYC.

We correspondingly developed a mathematical model including a system of differential equations and used the model to compute the level of miR-9 overexpression and let-7 downexpression in the setting of EGFR mutations and Ras mutations. We showed that such mutations upregulate the level of miR-9 and downregulate the level of let-7. The 25-fold increase in miR-9 levels obtained in the simulations was consistent quantitatively with clinical data reported in human lung tumors (Supplementary Material S1). Our experiments with EGFR mutant lung cancer cells did not show any significant changes in let-7 suggesting that let-7 may also be regulated by other signaling networks. We investigated how random perturbations of let-7 and miR-9 affect MMP and concluded that MMP is more robust against let-7 perturbations than against miR-9 perturbations; this can be explained by the fact that let-7 perturbations undergo damping by the negative feedbacks from let-7 to Ras and from ERK to SOS.

To the best of our knowledge, the present paper is the first one that develops a model for lung cancer and miRNA in terms of differential equations. The model is based on a signaling pathway that includes miR-9 and let-7. Simulations of the model demonstrate how mutations that are detected in NSCLC include upregulation of miR-9 and downregulation of let-7. The mathematical model could be further extended by including additional signaling pathways, specifically involving let-7, that are associated with lung cancer. However, an important next step in this line of investigation is to determine how deregulation of miR-9 and let-7 may jointly contribute to lung cancer progression and may be used as reliable biomarkers. In order to address this challenge mathematically, additional clinical investigation will be required.

Methods

In this model, we assume that the EGF-EGFR complex is at steady state and set it as a constant. Brown et al. (2004) modeled EGFR signaling with negative feedback of ERK to SOS [32]. We simplified some parts of their model to obtain the equations for SOS, Ras, and ERK. We denote by S, S_i, and S_{tot} the concentrations of active SOS, inactive SOS, and total SOS, respectively. Assuming that the total number of SOS is conserved, we have

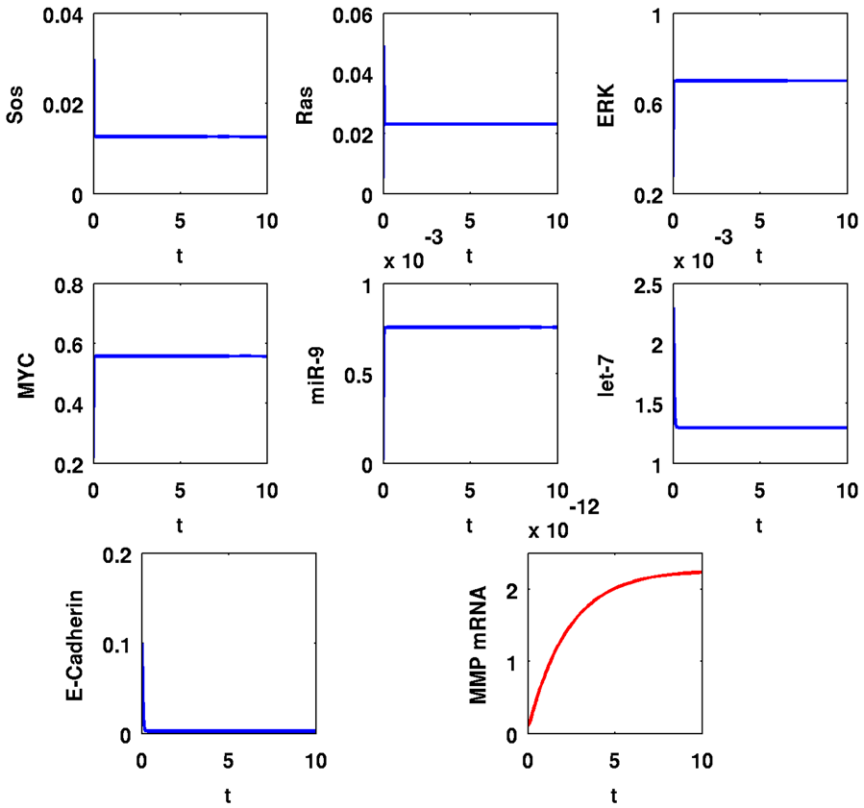

Figure 8. Simulation results for a cancer cell with Ras mutations, $\mu_R = 10\mu_{R0}$**.** Time is from $t = 0$ min to $t = 10^5$ min; initial values are those of a normal healthy cell; the units on the vertical axes are in μM and the units on the horizontal axes are scaled in 10^4 minutes.
doi:10.1371/journal.pone.0053663.g008

$$S + S_i = S_{tot}. \tag{9}$$

We denote by m_s the activation rate of the inactive SOS and by d_s as the deactivation rate of the active SOS. Describing these conversions by the Michaelis-Menten kinetics, the governing equation for the concentration of the active SOS is given by

$$\frac{dS}{dt} = m_s \cdot \frac{S_i}{S_i + K_{S1}} - d_s \cdot \frac{S}{S + K_{S2}}.$$

Using the fact that the EGF-EGFR complex activates SOS and that ERK represses active SOS, we replace m_s by $\mu_S E$ and d_s by $\delta_S Ek$, and we get Eq. (1). Similarly, we describe conversions between active and inactive Ras and between active and inactive ERK using Michaelis-Menten kinetics, and derive Eqs. (2) and (3). Here, catalytic activation rates of Ras and ERK are proportional to active SOS and active Ras concentrations, respectively. In Eq. (2), repression by let-7 of the activation of Ras is described by an inhibition factor, $K_{R2}/(L + K_{R2})$. In Eq. (4), production of MYC is proportional to active ERK concentration. In Eq. (5), activation of miR-9 by MYC is described by the fourth-order Hill function, since MYC is a transcription factor and miR-9 activation may involve several enzymatic steps. In Eq. (6), let-7 production is inhibited by MYC. In Eq. (7), E-Cadherin production is proportional to let-7 concentration and is inhibited by miR-9. Throughout Eqs. (4)–(7), degradation of species is described by linear mass action kinetics. Finally, in Eq. (8) MMP is produced at constant rate and is degraded by E-Cadherin.

The parameters of Eqs. (1)–(8) are derived in the following subsections. Most of the parameters are taken from Brown et al. (2004) [32]. In their model, they have taken the initial concentrations of all active signaling species to be zero, and the initial concentrations of all inactive signaling species to be $1\,\mu M$ except for MEK and ERK, whose concentrations were taken to be $5\,\mu M$. As for the EGF-EGFR complex concentration, Brown et al (2004) [32] assume it to be a variable but in our model, it is constant. This constant is chosen as the steady state concentration of the EGF-EGFR complex computed using their parameters.

Computation of E

We denote by X_e, X_r, and X_{er} the numbers of molecules of EGF, free EGFR, and EGF-EGFR complex, and by k_b and k_u the binding and unbinding rates for the EGF-EGFR complex. If X_0 is the total number of the EGFR molecules, then $X_r + X_{er} = X_0$. Assuming that binding and unbinding of EGF and EGFR are balanced at steady state, we have

$$k_b X_e (X_0 - X_{er}) - k_u X_{er} = 0,$$

which gives

$$X_{er} = \frac{k_b X_e X_0}{k_b X_e + k_u}. \tag{10}$$

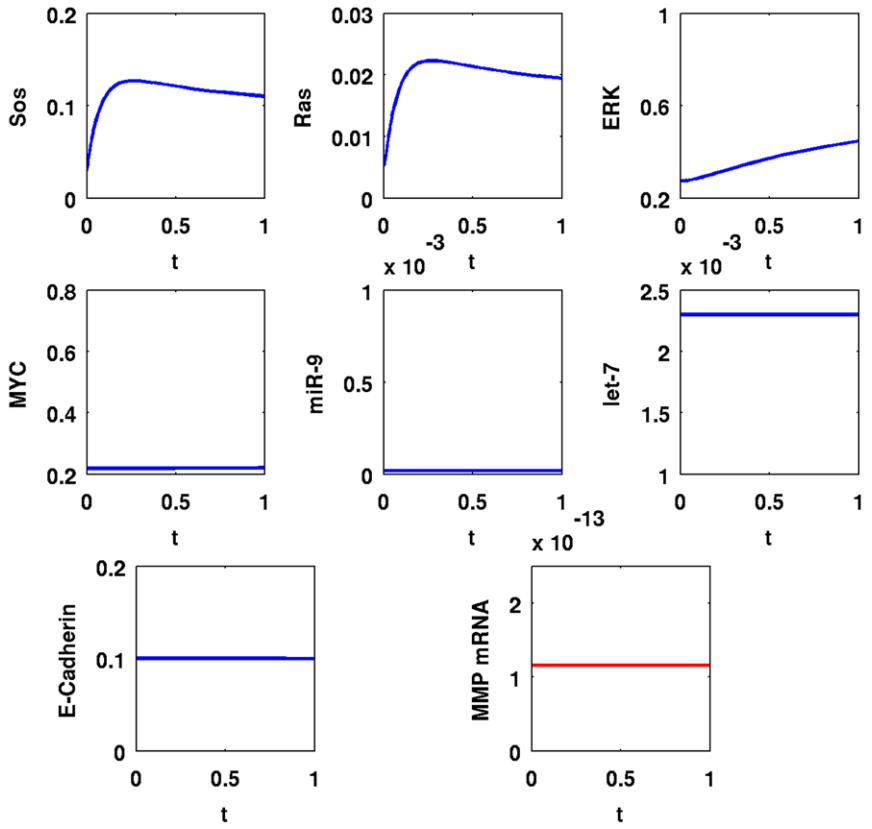

Figure 9. Simulation results for a cancer cell with disruption in the negative feedback from ERK to SOS, $\delta_S = \delta_{S0}/10$**.** Time is from $t = 0$ min to $t = 1$ min; initial values are those of a normal healthy cell; the units on the vertical axes are in μM and the units on the horizontal axes are in minutes.
doi:10.1371/journal.pone.0053663.g009

According to Brown et al. (2004) [32],

$$k_b = 2.18503 \times 10^{-5}/\text{min}$$

$$k_u = 0.0121008/\text{min}$$

$$X_e = 1.0002 \times 10^7$$

$$X_0 = 80000.0,$$

and hence $X_{er} = 79996.0$. We shall determine E by converting X_{er} into a unit of concentration. Lung cells size, however, vary up to 6-fold differences [39]. We therefore use an "average" cell size by taking it to be the HeLa cell.

Since EGF and EGFR are located on the cell surface, we need to compute the cell surface area; we assume that the cells have spherical shape with radius R. For HeLa cell, the total volume is

$$940\,\mu m^3 \text{ (volume of the cytoplasm)} +$$
$$220\,\mu m^3 \text{ (volume of the nucleus)}$$
$$= 1160\,\mu m^3 = \frac{4\pi R^3}{3},$$

according to Fujioka et al. (2006) [40]. Hence $R = 6.52\,\mu m$ and its surface area is

$$S = 4\pi R^2 = 533.89\,\mu m^2.$$

Converting the number of molecules of X_{er} into concentration on the cell surface, we compute steady-state concentration of EGF-EGFR complex as

$$E = \frac{X_{er}}{N_A S} = \frac{79996.0}{6.022 \times 10^{23}\,mol^{-1} \times 533.89\,\mu m^2}$$
$$= 0.2488\,\mu M \cdot \mu m$$

where N_A is the Avogadro's number, $6.022 \times 10^{23}\,mol^{-1}$; $1\,mol$ is the amount of a substance that contains as many entities as there are atoms in $12\,g$ of ^{12}C, and $1\,M$ is 1 molar concentration (per liter),

$$1\,M = 1\,mol/L = 1\,mol/dm^3.$$

Other parameters in the SOS equation

Let X_{Sa} and X_{Si} denote the numbers of active and inactive SOS molecules. According to Brown et al. (2004),

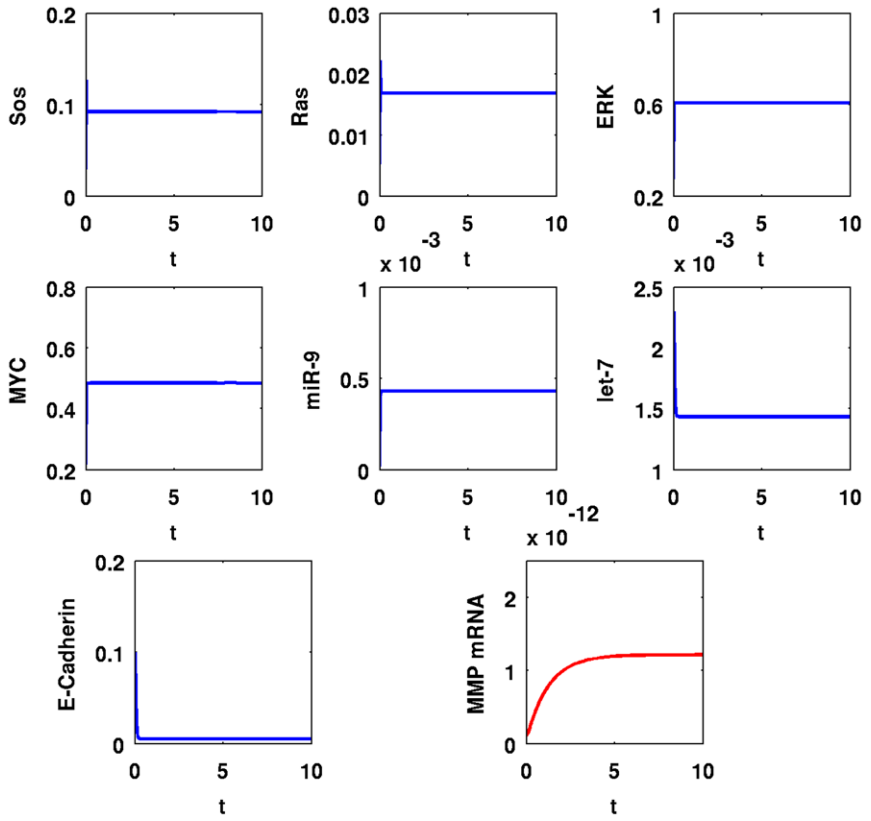

Figure 10. Simulation results for a cancer cell with disruption in the negative feedback from ERK to SOS, $\delta_S = \delta_{S0}/10$**.** Time is from $t = 0$ min to $t = 10^5$ min; initial values are those of a normal healthy cell; the units on the vertical axes are in μM and the units on the horizontal axes are scaled in 10^4 minutes.
doi:10.1371/journal.pone.0053663.g010

$$\frac{dX_{Sa}}{dt} = k_s X_{er} \cdot \frac{X_{Si}}{X_{Si} + K_{s1}} - d_s X_{P90Rska} \cdot \frac{X_{Sa}}{X_{Sa} + K_{s2}} \qquad (11)$$

where P90Rsk is a p90 ribosomal s6 kinase that inactivates SOS, and $X_{P90Rska}$ is the number of active P90Rsk molecules [32]. In that paper, parameters are given as $k_s = 694.731/\text{min}$, $K_{s1} = 6086070.0$, $d_s = 1611.97/\text{min}$, and $K_{s2} = 896896.0$. Using these numbers, we determine our parameters by

$$K_{S1} = \frac{K_{s1}}{N_A V_c} = 10.7515\,\mu M$$

$$K_{S2} = \frac{K_{s2}}{N_A V_c} = 1.5844\,\mu M$$

$$\mu_S = k_s \times \frac{N_A S}{N_A V_c} = 394.5868/(\mu m \cdot \text{min}),$$

where $V_c = 940\,\mu m^3$ is the volume of the cytoplasm in a HeLa cell. The total number of molecules of active P90Rsk was taken to be 120,000.0 [32]. Since the initial concentration of ERK, $5\,\mu M$, corresponds to 600,000.0 molecules, we get

$$\delta_S = d_s \times \frac{120{,}000.0}{600{,}000.0} = 322.3940/\text{min}.$$

The initial concentration of SOS (all inactive) was $1\,\mu M$, which corresponds to 120,000.0 molecules. We convert this number to concentration using the volume of the cytoplasm in a HeLa cell,

$$S_{tot} = \frac{120{,}000.0}{N_A V_c} = 0.2120\,\mu M.$$

Parameters in the Ras equation

Let X_{Ra} and X_{Ri} denote the numbers of molecules of active and inactive Ras. From Brown et al. (2004),

$$\frac{dX_{Ra}}{dt} = k_r X_{Sa} \cdot \frac{X_{Ri}}{X_{Ri} + K_{r1}} - d_r X_{RGa} \cdot \frac{X_{Ra}}{X_{Ra} + K_{r2}} \qquad (12)$$

where X_{Sa} and X_{RGa} denote the numbers of molecules of active SOS and active Ras-Gap [32]. In [32], parameters are given as $k_r = 32.344/\text{min}$, $K_{r1} = 35954.3$, $d_r = 1509.36/\text{min}$, and $K_{r2} = 1432410.0$. Also, the number of molecules of active Ras-Gap is treated as a constant equal to 120,000.0. Accordingly, we determine our parameters by

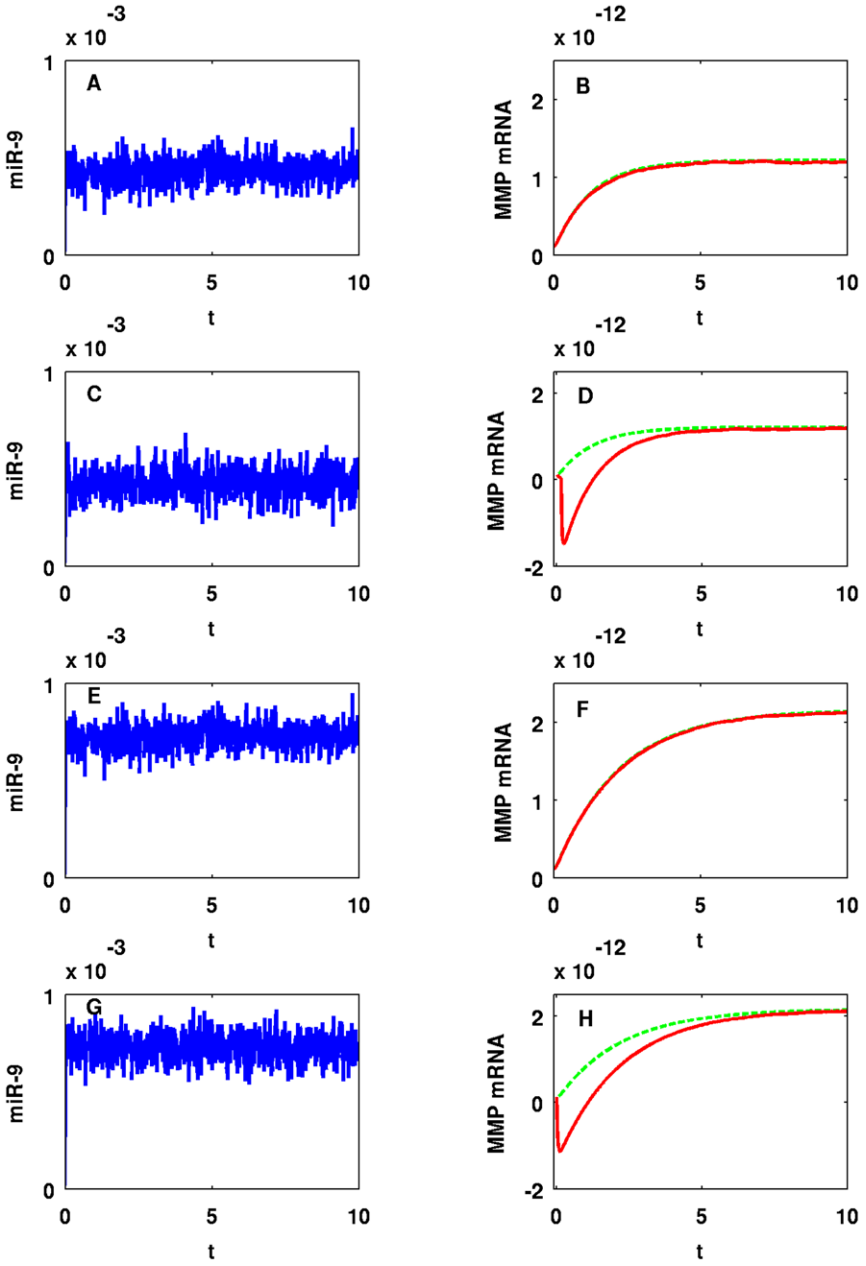

Figure 11. One sample path of miR-9 and MMP concentrations in time with random input in miR-9. For (A–D) $E=10E_0$ and for (E–H) $E=20E_0$. For (A, B, E, F) $\sigma=10^{-5}$ and for (C, D, G, H) $\sigma=1.2\times10^{-5}$. The units on the horizontal axes are scaled in 10^4 minutes.
doi:10.1371/journal.pone.0053663.g011

$$K_{R1}=\frac{K_{r1}}{N_A V_c}=0.0635\,\mu M$$

$$K_{R3}=\frac{K_{r2}}{N_A V_c}=2.5305\,\mu M$$

$$\mu_R=k_r=32.344\,/\mathrm{min}$$

$$\delta_R=d_r\times\frac{X_{RGa}}{N_A V_c}=319.9672\,\mu M/\mathrm{min}.$$

For total Ras concentration, we convert the total number of Ras molecules in a cell obtained from [32] to concentration using the volume of the cytoplasm in a HeLa cell,

$$R_{tot}=\frac{120{,}000.0}{N_A V_c}=0.2120\,\mu M.$$

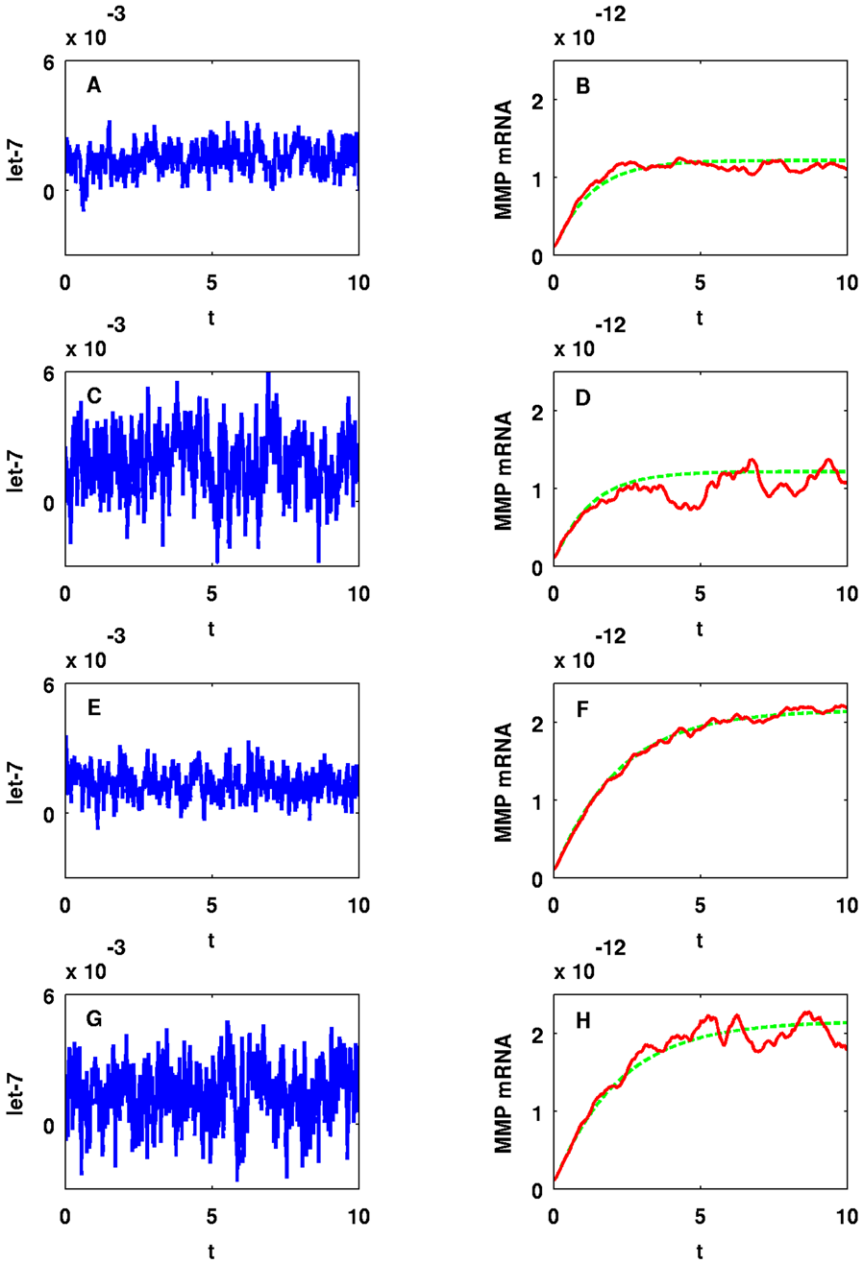

Figure 12. One sample path of let-7 and MMP concentrations in time with random input in let-7. For (A–D) $E=10E_0$ and for (E–H) $E=20E_0$. For (A, B, E, F) $\sigma=5\times10^{-5}$ and for (C, D, G, H) $\sigma=10^{-4}$. The units on the horizontal axes are scaled in 10^4 minutes.
doi:10.1371/journal.pone.0053663.g012

Parameters in the ERK equation

Let X_{Eka} and X_{Eki} denote the numbers of molecules of active and inactive ERK. Following Brown et al. (2004),

$$\frac{dX_{Eka}}{dt}=k_{ek}X_{Ma}\cdot\frac{X_{Eki}}{X_{Eki}+K_{ek1}}-d_{ek}X_{Pa}\cdot\frac{X_{Eka}}{X_{Eka}+K_{ek2}} \quad (13)$$

where X_{Ma} and X_{Pa} denote the numbers of molecules of active MEK and active PP2A [32]. PP2A is protein phosphatase 2 which is an enzyme targeting proteins in oncogenic signaling pathways. In that paper, parameters are given as $k_{ek}=9.85367/\text{min}$, $K_{ek1}=1007340.0$, $d_{ek}=8.8912/\text{min}$, and $K_{ek2}=3496490.0$; the initial total numbers of molecules of MEK and Ras are given as 600,000.0 and 120,000.0, and the number of molecules of active PP2A is treated as a constant equal to 120,000.0. Therefore, we determine our parameters by

$$K_{Ek1}=\frac{K_{ek1}}{N_AV_c}=1.7795\,\mu M$$

$$K_{Ek2}=\frac{K_{ek2}}{N_AV_c}=6.1768\,\mu M$$

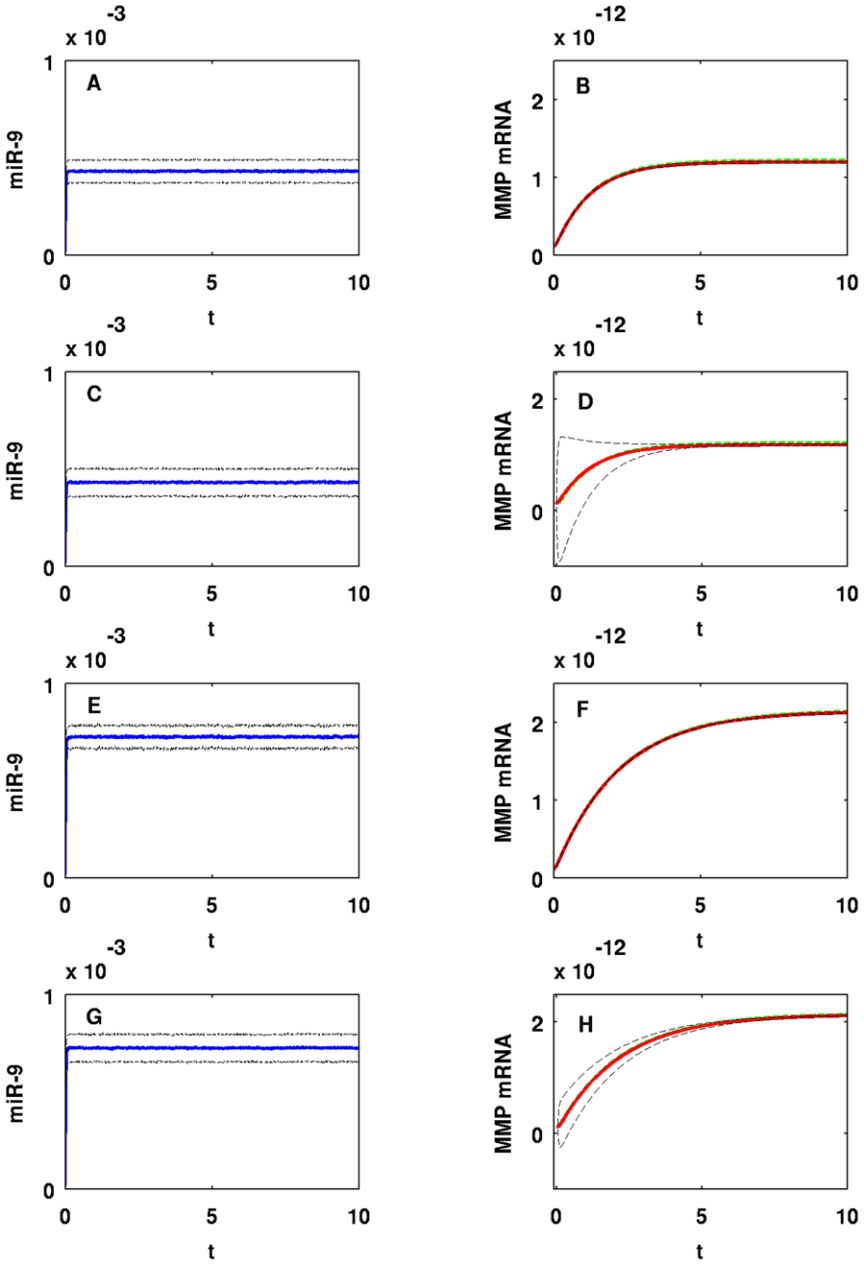

Figure 13. Mean concentrations of miR-9 and MMP and standard deviations from the means in time with random input in miR-9. For (A–D) $E=10E_0$ and for (E–H) $E=20E_0$. For (A, B, E, F) $\sigma=10^{-5}$ and for (C, D, G, H) $\sigma=1.2\times10^{-5}$. The units on the horizontal axes are scaled in 10^4 minutes. The result is taken from 1,000 realizations of simulation.
doi:10.1371/journal.pone.0053663.g013

$$\mu_{Ek}=k_{ek}\times\frac{600{,}000.0}{120{,}000.0}=49.2683\,/\mathrm{min}$$

$$\delta_{Ek}=d_{ek}\times\frac{X_{Pa}}{N_A V_c}=1.8848\,\mu M/\mathrm{min}.$$

We convert the total number of ERK molecules, consisting of active and inactive ERK in a cell to concentration, using the volume of the cytoplasm in a HeLa cell, and set

$$Ek_{tot}=\frac{600{,}000.0}{N_A V_c}=1.0599\,\mu M.$$

Parameters in the MYC equation

Following Rudolph et al. (1999), there are 29,000 c-MYC proteins in the nucleus [41]. We convert this to concentration using the volume of the nucleus in a HeLa cell, $V_n=220\,\mu m^3$. Treating this concentration as the steady-state concentration of MYC, we get

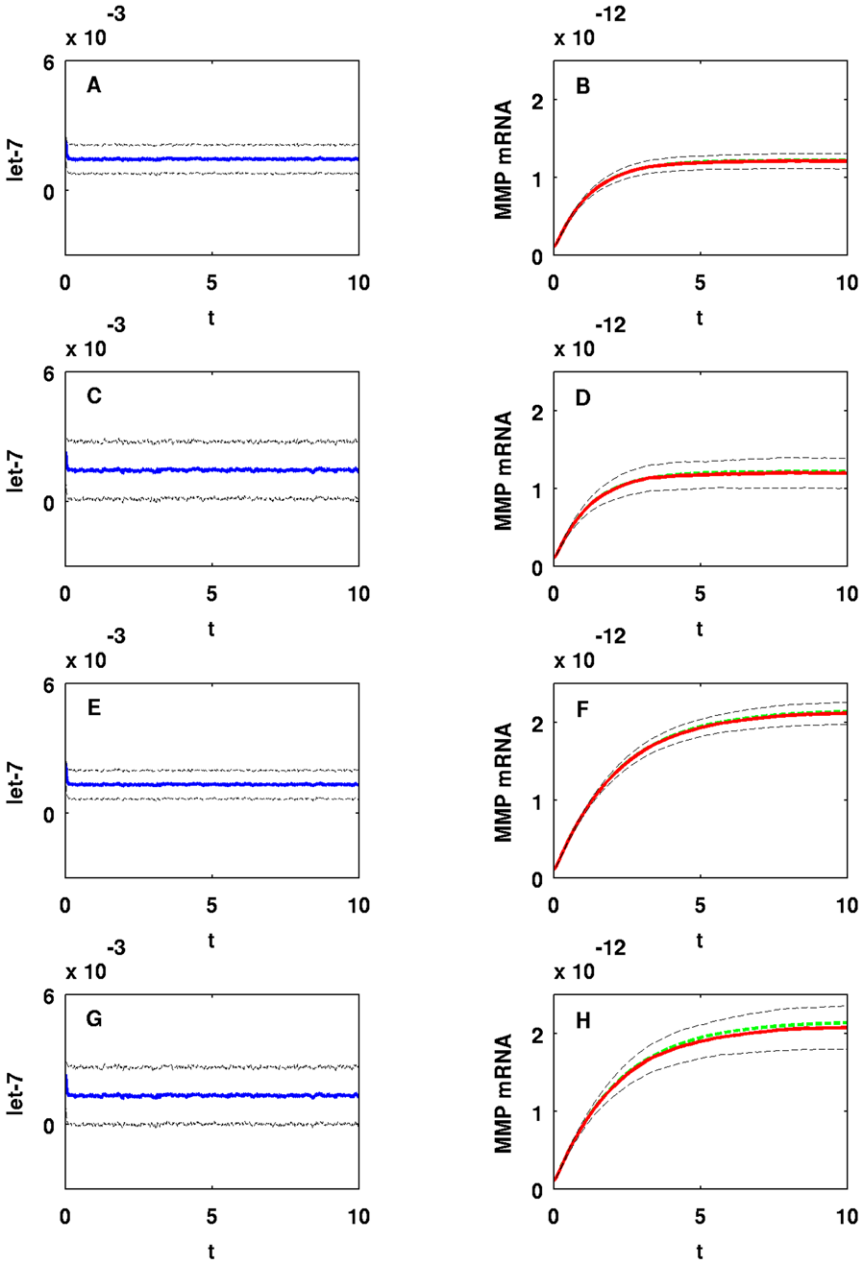

Figure 14. Mean concentrations of let-7 and MMP and standard deviations from the means in time with random input in let-7. For (A–D) $E=10E_0$ and for (E–H) $E=20E_0$. For (A, B, E, F) $\sigma=5\times10^{-5}$ and for (C, D, G, H) $\sigma=10^{-4}$. The units on the horizontal axes are scaled in 10^4 minutes. The result is taken from 1,000 realizations of simulation.
doi:10.1371/journal.pone.0053663.g014

$$C_0=\frac{29{,}000}{N_A V_n}=0.2189\,\mu M.$$

Half-life of c-MYC protein is $15-50\,min$ [42]. We take the half-life of c-MYC as $30/\min$, and compute a degradation rate as

$$\delta_C=\frac{\ln 2}{30\,\min}=0.0231/\min.$$

In steady state in Eq. (4),

$$0=\mu_C Ek_0-\delta_C C_0 \tag{14}$$

where Ek_0 is the steady-state concentration of ERK. To determine Ek_0, we first compute steady-state concentration of let-7. Following Lim et al. (2003), there are 1300 let-7 molecules in a human HeLa cell [43], and we assume that this number is at steady state. We convert it to concentration by

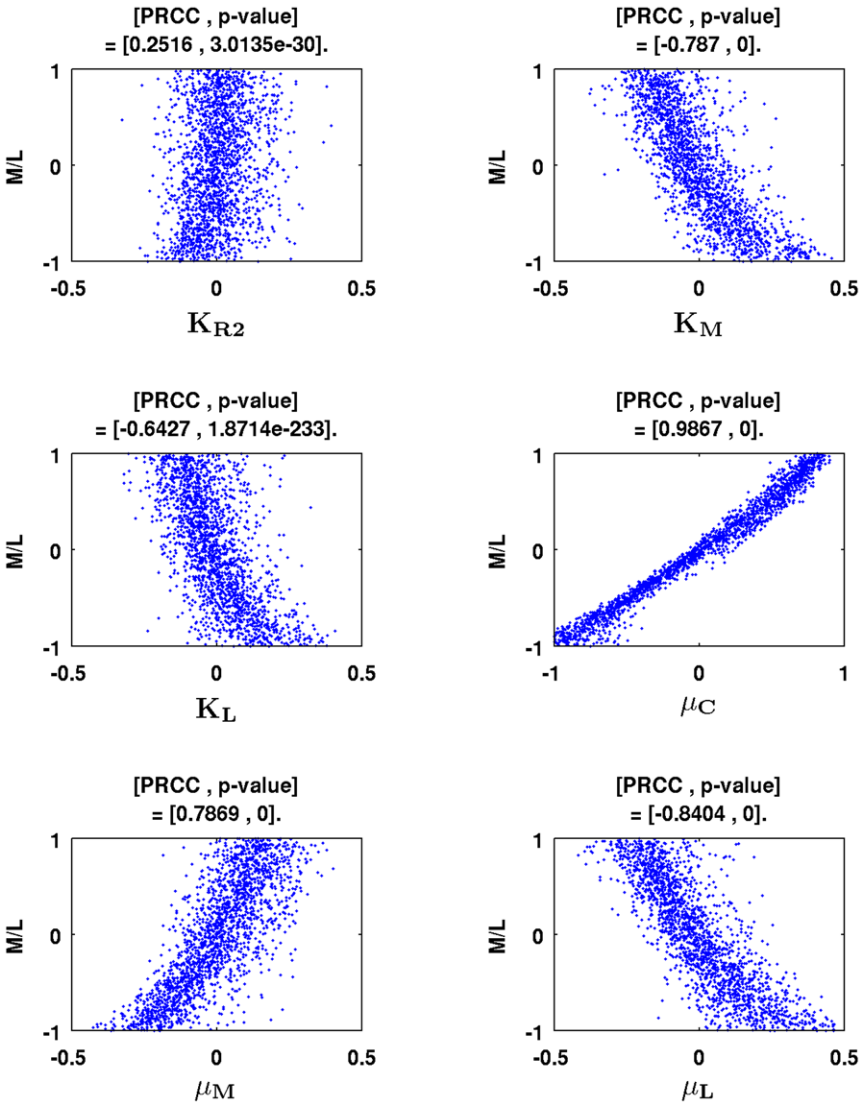

Figure 15. Scatter plots of rank transformed M/L with several rank transformed parameters. Scatter plots are drawn for statistically significant parameters (p-value <0.01); the units on the horizontal and vertical axes are scaled in 1,000; time is at 10^5 minutes and the result is taken from 2,000 realizations of simulation.
doi:10.1371/journal.pone.0053663.g015

$$L_0 = \frac{1300}{N_A V_c} = 0.0023\,\mu M.$$

We compute a solution of Eq. (1)–(3) for S, R, and Ek with L replaced by L_0 using Matlab, and obtain the steady-state concentration of ERK as $Ek_0 = 0.2746\,\mu M$. From Eq. (14), we then get

$$\mu_C = \frac{\delta_C C_0}{Ek_0} = 0.0184\,/\mathrm{min}.$$

Parameters in the miR-9 equation

Since the miR-9 copy number in the normal lung cell is very small [44], we take the steady-state concentration of miR-9 to be $M_0 = 1.8 \times 10^{-5}\,\mu M$. Half-life of miR-9 in human brain tissue is $0.8\,hour$ [45], which gives the degradation rate $\delta_M = 0.0144\,/\mathrm{min}$. In steady state in Eq. (5),

$$0 = \mu_M \frac{C_0^4}{C_0^4 + K_M} - \delta_M M_0.$$

Based on the fact that miR-9 expression in the NSCLC tissues is about $20-30$ times that of normal tissues (see Supplementary Material S1), we take K_M to be very large, namely, $K_M = 10{,}000 C_0^4$. Then

$$\mu_M = \frac{\delta_M M_0}{1/10001} = 0.0026\,\mu M/\mathrm{min}.$$

Table 2. Summary of the parameter values.

Name	Description	Value used	References
E_0	concentration of EGF-EGFR complex (constant)	$0.2488\,\mu M\cdot\mu m$	[32]
S_{tot}	total concentration of SOS	$0.2120\,\mu M$	[32]
R_{tot}	total concentration of Ras	$0.2120\,\mu M$	[32]
Ek_{tot}	total concentration of ERK	$1.0599\,\mu M$	[32]
S_0	Steady-state concentration of active SOS	$0.0298\,\mu M$	estimated
R_0	Steady-state concentration of active Ras	$0.0053\,\mu M$	estimated
Ek_0	Steady-state concentration of active ERK	$0.2746\,\mu M$	estimated
C_0	Steady-state concentration of MYC protein	$0.2189\,\mu M$	[41]
M_0	Steady-state concentration of miR-9	$1.8\times10^{-5}\,\mu M$	estimated
L_0	Steady-state concentration of let-7	$0.0023\,\mu M$	[43]
H_0	Steady-state concentration of E-Cadherin	$0.1\,\mu M$	[47]
P_0	Steady-state concentration of MMP mRNA	$1.1574\times10^{-13}\,\mu M$	[49]
K_{S1}	Saturation of inactive SOS on active SOS	$10.7515\,\mu M$	[32]
K_{S2}	Saturation of active SOS on inactive SOS	$1.5844\,\mu M$	[32]
K_{R1}	Saturation of inactive Ras on active Ras	$0.0635\,\mu M$	[32]
K_{R2}	Control of let-7 on Ras	$0.0230\,\mu M$	estimated
K_{R3}	Saturation of active Ras on inactive Ras	$2.5305\,\mu M$	[32]
K_{Ek1}	Saturation of inactive ERK on active ERK	$1.7795\,\mu M$	[32]
K_{Ek2}	Saturation of active ERK on inactive ERK	$6.1768\,\mu M$	[32]
K_M	Saturation of MYC on miR-9	$22.9606\,\mu M^4$	estimated
K_L	Control of MYC on let-7	$0.2189\,\mu M$	estimated
K_H	Control of MYC on E-Cadherin	$1.8\times10^{-5}\,\mu M$	estimated
K_P	Control of E-Cadherin on MMP mRNA	$0.1\,\mu M$	estimated
μ_S	Catalytic production rate of active SOS	$394.5868\,/(\mu m\cdot\min)$	[32]
μ_{R0}	Catalytic production rate of active Ras	$32.344\,/\min$	[32]
μ_{Ek}	Catalytic production rate of active ERK	$49.2683\,/\min$	[32]
μ_C	Catalytic production rate of MYC	$0.0184\,/\min$	estimated
μ_M	Catalytic production rate of miR-9	$0.0026\,\mu M/\min$	estimated
μ_L	Catalytic production rate of let-7	$1.3340\times10^{-5}\,\mu M/\min$	estimated
μ_H	Catalytic production rate of E-Cadherin	$0.2087\,/\min$	estimated
μ_P	Catalytic production rate of MMP	$9.8379\times10^{-17}\,\mu M/\min$	estimated
δ_{S0}	Degradation rate of active SOS	$322.3940\,/\min$	[32]
δ_R	Degradation rate of active Ras	$319.9672\,\mu M/\min$	[32]
δ_{Ek}	Degradation rate of active ERK	$1.8848\,\mu M/\min$	[32]
δ_C	Degradation rate of MYC protein	$0.0231\,/\min$	[42]
δ_M	Degradation rate of miR-9	$0.0144\,/\min$	[45]
δ_L	Degradation rate of let-7	$0.0029\,/\min$	[46]
δ_H	Degradation rate of E-Cadherin	$0.0024\,/\min$	[48]
δ_P	Degradation rate of MMP mRNA	$0.0017\,/\min$	[51]

The table summarizes all the parameter values of the model equations (1)–(8).
doi:10.1371/journal.pone.0053663.t002

Parameters in the let-7 equation

Half-life of let-7 after TAM treatment is $4\,hours$ [46]. Accordingly, we take the degradation rate of $\delta_L=0.0029\,/\min$. Then, in steady state in Eq. (6),

$$0=\mu_L\frac{K_L}{C_0+K_L}-\delta_L L_0.$$

Table 3. Parameter ranges and partial rank correlation coefficient (PRCC) values.

Parameter	Range	PRCC
S_0	$[0.0149,0.0596]\,\mu M$	0.0072
R_0	$[0.0027,0.0106]\,\mu M$	0.0084
Ek_0	$[0.1373,0.5492]\,\mu M$	0.0178
M_0	$[0.0900,0.3600]10^{-4}\,\mu M$	0.0027
K_{R2}	$[0.0115,0.0460]\,\mu M$	0.2516*
K_M	$[11.4803,45.9212]\,\mu M^4$	−0.7870*
K_L	$[0.1095,0.4378]\,\mu M$	−0.6427*
K_H	$[0.0900,0.3600]10^{-4}\,\mu M$	0.0294
K_P	$[0.0500,0.2000]\,\mu M$	−0.0397
μ_C	$[0.0092,0.0368]$/min	0.9867*
μ_M	$[0.0013,0.0052]\,\mu M$/min	0.7869*
μ_L	$[0.0667,0.2668]10^{-4}\,\mu M$/min	−0.8404*
μ_H	$[0.1043,0.4174]$/min	−0.0283
μ_P	$[0.0492,0.1968]10^{-15}\,\mu M$/min	−0.0231

Statistically significant parameters are denoted as * (p-value <0.01).
doi:10.1371/journal.pone.0053663.t003

Taking $K_L = C_0$ gives

$$\mu_L = \frac{\delta_L L_0}{1/2} = 1.3340 \times 10^{-5}\,\mu M/\text{min}.$$

Parameters in the E-Cadherin equation

Using the total E-Cadherin concentration in Chaplain (2011) [47], we set steady-state concentration, $H_0 = 100nM = 0.1\,\mu M$. Half-life of E-Cadherin is 4.8 *hours* [48], so the degradation rate is $\delta_H = 0.0024/\text{min}$. In steady state in Eq. (7),

$$0 = \mu_H L_0 \frac{K_H}{M_0 + K_H} - \delta_H H_0.$$

Taking $K_H = M_0$ gives

$$\mu_H = \frac{\delta_H H_0}{1/2L_0} = 0.2087/\text{min}.$$

Parameters in the MMP mRNA equation

According to Safranek et al. (2009), the number of MMP-9 mRNA in human lung tissue is $20.50/100mg$ [49]. Using the human lung tissue density of $0.34g/cm^3$ [50], we compute the MMP mRNA concentration in steady state,

$$P_0 = 20.50/100mg \times 0.34g/cm^3 \times \frac{1}{6.022 \times 10^{23} mol^{-1}} = 1.1574 \times 10^{-13}\,\mu M.$$

Half-life of MMP-9 mRNA is 7 *hours* [51], so the degradation rate is $\delta_P = 0.0017/\text{min}$. Using the steady state equation for MMP concentration,

$$0 = \mu_P - \frac{H_0}{H_0 + K_P}\delta_P P_0,$$

and taking $K_P = H_0$, we get

$$\mu_P = \frac{1}{2}\delta_P P_0 = 9.8379 \times 10^{-17}\,\mu M/\text{min}.$$

Cell culture and drug treatment

For our experiments shown in Figure 16, we obtained the EGFR mutant lung cancer cell line (HCC827) (E746-A750 deletion) as a generous gift from our collaborator (Michela Garofalo, OSU). Cells were maintained in appropriate media. HCC827 cell lines were subsequently treated with Gefitinib (generous gift from Michela Garofalo, OSU) at concentrations of $1\,\mu M$, $5\,\mu M$, and $10\,\mu M$. Following 24 hours of exposure, cells were harvested for RNA and assessed for miR-9 (Assay ID# Hs000583), let-7a (Assay ID# Hs00377), c-MYC (Assay ID# Hs00153408_m1) (Applied Biosystems) by QRT-PCR. For miRNA assessment RNU48 was used as the endogenous control and for c-MYC GAPDH was used. Data is presented as fold difference based on $2^{-\Delta Ct}$. Statistical analyses were performed using ANOVA with Tukey Post Hoc analysis.

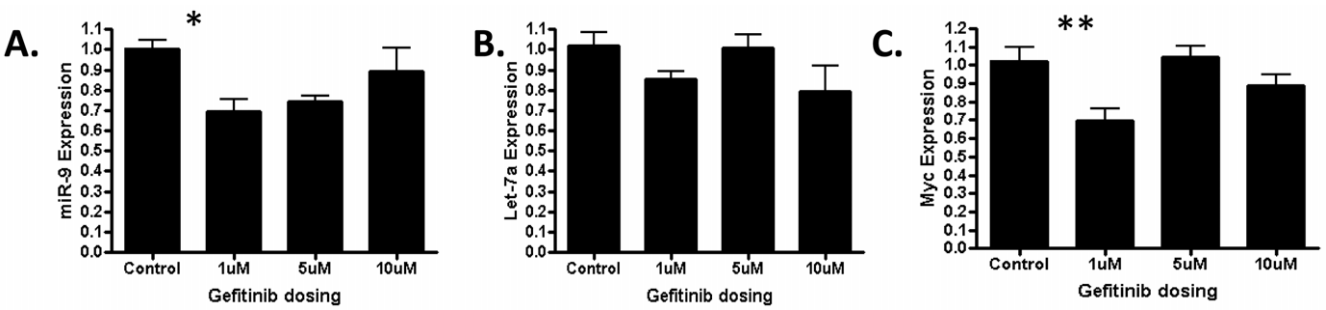

Figure 16. QRT-PCR expression of miR-9, let-7a and c-MYC in HCC827 lung cancer cell lines treated with Gefitinib. Statistical significance is defined as *$p<0.05$ in (A) and **$p<0.01$ in (C).
doi:10.1371/journal.pone.0053663.g016

Supporting Information

Material S1 Experimental results of miR-9 in lung tumor tissues. Experimental results using quantitative reverse transcription polymerase chain reaction and in situ hybridization for miR-9 are provided.
(PDF)

Author Contributions

Conceived and designed the experiments: HWK AF SPNS. Performed the experiments: MC GN HWK. Analyzed the data: HWK AF SPNS. Contributed reagents/materials/analysis tools: MF SPNS. Wrote the paper: HWK AF SPNS. Provided lung tumor tissues for the PCR experiments: MF. Provided EGFR mutant lung cancer cell lines and Gefitinib: MG.

References

1. Siegel R, Naishadham D, Jemal A (2012) Cancer statistics, 2012. CA: A Cancer Journal for Clinicians.
2. Takamizawa J, Konishi H, Yanagisawa K, Tomida S, Osada H, et al. (2004) Reduced expression of the let-7 microRNAs in human lung cancers in association with shortened postoperative survival. Cancer Research 64: 3753.
3. Nicoloso M, Spizzo R, Shimizu M, Rossi S, Calin G (2009) MicroRNAs-the micro steering wheel of tumour metastases. Nature Reviews Cancer 9: 293–302.
4. Trang P, Medina P, Wiggins J, Ruffino L, Kelnar K, et al. (2009) Regression of murine lung tumors by the let-7 microRNA. Oncogene 29: 1580–1587.
5. Trang P, Wiggins J, Daige C, Cho C, Omotola M, et al. (2011) Systemic delivery of tumor suppressor microrna mimics using a neutral lipid emulsion inhibits lung tumors in mice. Molecular Therapy 19: 1116–1122.
6. Yanaihara N, Caplen N, Bowman E, Seike M, Kumamoto K, et al. (2006) Unique microRNA molecular profiles in lung cancer diagnosis and prognosis. Cancer Cell 9: 189–198.
7. Volinia S, Calin G, Liu C, Ambs S, Cimmino A, et al. (2006) A microRNA expression signature of human solid tumors defines cancer gene targets. Proceedings of the National Academy of Sciences of the United States of America 103: 2257.
8. Crawford M, Batte K, Yu L, Wu X, Nuovo G, et al. (2009) MicroRNA 133B targets pro-survival molecules MCL-1 and BCL2L2 in lung cancer. Biochemical and Biophysical Research Communications 388: 483–489.
9. Võsa U, Vooder T, Kolde R, Fischer K, Välk K, et al. (2011) Identification of miR-374a as a prognostic marker for survival in patients with early-stage nonsmall cell lung cancer. Genes, Chromosomes and Cancer.
10. Ma L, Young J, Prabhala H, Pan E, Mestdagh P, et al. (2010) miR-9, a MYC/MYCN-activated microRNA, regulates E-cadherin and cancer metastasis. Nature Cell Biology 12: 247–256.
11. Mascaux C, Laes J, Anthoine G, Haller A, Ninane V, et al. (2009) Evolution of microRNA expression during human bronchial squamous carcinogenesis. European Respiratory Journal 33: 352.
12. Frenzel A, Lovén J, Henriksson M (2010) Targeting MYC-regulated miRNAs to combat cancer. Genes & Cancer 1: 660.
13. Aguda B, Kim Y, Piper-Hunter M, Friedman A, Marsh C (2008) MicroRNA regulation of a cancer network: consequences of the feedback loops involving miR-17-92, E2F, and Myc. Proceedings of the National Academy of Sciences of the United States of America 105: 19678.
14. Yokota J, Wada M, Yoshida T, Noguchi M, Terasaki T, et al. (1988) Heterogeneity of lung cancer cells with respect to the amplification and rearrangement of myc family oncogenes. Oncogene 2: 607.
15. Broers J, Viallet J, Jensen S, Pass H, Travis W, et al. (1993) Expression of c-myc in progenitor cells of the bronchopulmonary epithelium and in a large number of non-small cell lung cancers. American Journal of Respiratory Cell and Molecular Biology 9: 33.
16. Rapp U, Korn C, Ceteci F, Karreman C, Luetkenhaus K, et al. (2009) MYC is a metastasis gene for non-small-cell lung cancer. PLoS One 4: e6029.
17. Rinaldi A, Poretti G, Kwee I, Zucca E, Catapano C, et al. (2007) Concomitant MYC and microRNA cluster miR-17-92 (C13orf25) amplification in human mantle cell lymphoma. Leukemia & Lymphoma 48: 410.
18. Wolfer A, Ramaswamy S (2011) MYC and metastasis. Cancer Research 71: 2034.
19. Inamura K, Togashi Y, Nomura K, Ninomiya H, Hiramatsu M, et al. (2007) let-7 microRNA expression is reduced in bronchioloalveolar carcinoma, a non-invasive carcinoma, and is not correlated with prognosis. Lung Cancer 58: 392–396.
20. Wang Z, Lin S, Li J, Xu Z, Yao H, et al. (2011) MYC protein inhibits transcription of the microRNA cluster MC-let-7a-1 – let-7d via noncanonical e-box. Journal of Biological Chemistry 286: 39703–39714.
21. Johnson S, Grosshans H, Shingara J, Byrom M, Jarvis R, et al. (2005) RAS is regulated by the let-7 microRNA family. Cell 120: 635–647.
22. Lee Y, Dutta A (2007) The tumor suppressor microRNA let-7 represses the HMGA2 oncogene. Genes & Development 21: 1025–1030.
23. Thuault S, Tan E, Peinado H, Cano A, Heldin C, et al. (2008) HMGA2 and Smads co-regulate SNAIL1 expression during induction of epithelial-to-mesenchymal transition. Journal of Biological Chemistry 283: 33437.
24. Nawrocki-Raby B, Gilles C, Polette M, Bruyneel E, Laronze J, et al. (2003) Upregulation of MMPs by soluble E-cadherin in human lung tumor cells. International Journal of Cancer 105: 790–795.
25. Zheng S, Chang Y, Hodges K, Sun Y, Ma X, et al. (2010) Expression of KISS1 and MMP-9 in non-small cell lung cancer and their relations to metastasis and survival. Anticancer Research 30: 713–718.
26. Rao J, Gondi C, Chetty C, Chittivelu S, Joseph P, et al. (2005) Inhibition of invasion, angiogenesis, tumor growth, and metastasis by adenovirus-mediated transfer of antisense uPAR and MMP-9 in non–small cell lung cancer cells. Molecular Cancer Therapeutics 4: 1399.
27. Sulzer M, Leers M, van NOORD J, Bollen E, Theunissen P (1998) Reduced Ecadherin expression is associated with increased lymph node metastasis and unfa29 vorable prognosis in non-small cell lung cancer. American Journal of Respiratory and Critical Care Medicine 157: 1319–1323.
28. Mitselou A, Batistatou A, Nakanishi Y, Hirohashi S, Vougiouklakis T, et al. (2010) Comparison of the dysadherin and E-cadherin expression in primary lung cancer and metastatic sites. Histology and Histopathology 25: 1257–1267.
29. Saad A, Yeap B, Thunnissen F, Pinkus G, Pinkus J, et al. (2008) Immunohistochemical markers associated with brain metastases in patients with nonsmall cell lung carcinoma. Cancer 113: 2129–2138.
30. Roberts P, Der C (2007) Targeting the Raf-MEK-ERK mitogen-activated protein kinase cascade for the treatment of cancer. Oncogene 26: 3291–3310.
31. Zhao C, Du G, Skowronek K, Frohman M, Bar-Sagi D (2007) Phospholipase D2-generated phosphatidic acid couples EGFR stimulation to Ras activation by Sos. Nature Cell Biology 9: 707–712.
32. Brown K, Hill C, Calero G, Myers C, Lee K, et al. (2004) The statistical mechanics of complex signaling networks: nerve growth factor signaling. Physical Biology 1: 184.
33. Orton R, Adriaens M, Gormand A, Sturm O, Kolch W, et al. (2009) Computational modelling of cancerous mutations in the EGFR/ERK signalling pathway. BMC Systems Biology 3: 100.
34. Huang S, Ren X, Wang L, Zhang L, Wu X (2011) Lung-cancer chemoprevention by induction of synthetic lethality in mutant KRAS premalignant cells in vitro and in vivo. Cancer Prevention Research 4: 666.
35. Zhang Z, Stiegler A, Boggon T, Kobayashi S, Halmos B (2010) EGFR-mutated lung cancer: a paradigm of molecular oncology. Oncotarget 1: 497.
36. da Cunha Santos G, Shepherd F, Tsao M (2011) EGFR mutations and lung cancer. Annual Review of Pathology: Mechanisms of Disease 6: 49–69.
37. Adjei A (2001) Blocking oncogenic Ras signaling for cancer therapy. Journal of the National Cancer Institute 93: 1062–1074.
38. Marino S, Hogue I, Ray C, Kirschner D (2008) A methodology for performing global uncertainty and sensitivity analysis in systems biology. Journal of Theoretical Biology 254: 178–196.
39. Stone K, Mercer R, Gehr P, Stockstill B, Crapo J, et al. (1992) Allometric relationships of cell numbers and size in the mammalian lung. American Journal of Respiratory Cell and Molecular Biology 6: 235.
40. Fujioka A, Terai K, Itoh R, Aoki K, Nakamura T, et al. (2006) Dynamics of the Ras/ERK MAPK cascade as monitored by fluorescent probes. Journal of Biological Chemistry 281: 8917–8926.
41. Rudolph C, Adam G, Simm A (1999) Determination of copy number of c-Myc protein per cell by quantitative western blotting. Analytical Biochemistry 269: 66–71.
42. Luscher B, Eisenman R (1988) c-myc and c-myb protein degradation: effect of metabolic inhibitors and heat shock. Molecular and Cellular Biology 8: 2504.
43. Lim L, Lau N, Weinstein E, Abdelhakim A, Yekta S, et al. (2003) The microRNAs of Caenorhabditis elegans. Genes & Development 17: 991.
44. Liang Y, Ridzon D, Wong L, Chen C (2007) Characterization of microRNA expression profiles in normal human tissues. BMC Genomics 8: 166.
45. Sethi P, Lukiw W (2009) Micro-RNA abundance and stability in human brain: specific alterations in Alzheimer's disease temporal lobe neocortex. Neuroscience Letters 459: 100–104.
46. Iliopoulos D, Hirsch H, Struhl K (2009) An epigenetic switch involving NF-κ B, Lin28, let-7 microRNA, and IL6 links inflammation to cell transformation. Cell 139: 693–706.
47. Chaplain M (2011) Multiscale mathematical modelling in biology and medicine. IMA Journal of Applied Mathematics 76: 371.
48. Fujita Y, Krause G, Scheffner M, Zechner D, Leddy H, et al. (2002) Hakai, a c-Cbl-like protein, ubiquitinates and induces endocytosis of the E-cadherin complex. Nature Cell Biology 4: 222–231.
49. Safranek J, Pesta M, Holubec L, Kulda V, Dreslerova J, et al. (2009) Expression of MMP-7, MMP-9, TIMP-1 and TIMP-2 mRNA in lung tissue of patients with non-small cell lung cancer (NSCLC) and benign pulmonary disease. Anticancer Research 29: 2513.
50. Hopkins S, Henderson A, Levin D, Yamada K, Arai T, et al. (2007) Vertical gradients in regional lung density and perfusion in the supine human lung: the Slinky effect. Journal of Applied Physiology 103: 240–248.

51. Akool E, Kleinert H, Hamada F, Abdelwahab M, Forstermann U, et al. (2003) Nitric oxide increases the decay of matrix metalloproteinase 9 mRNA by inhibiting the expression of mRNA-stabilizing factor HuR. Molecular and Cellular Biology 23: 4901.